Inorg. Chem. **2008**, *47*, 5145−5153

pH-Dependent Assembly of Hybrids Based on Wells-Dawson POM/Ag Chemistry

Jingquan Sha,[†,‡] Jun Peng,[*,†] Yaqan Lan,[†] Zhongmin Su,[†] Haijun Pang,[†] Aixiang Tian,[†] Pengpeng Zhang,[†] and Min Zhu[†]

Key Laboratory of Polyoxometalate Science of Ministry of Education, Faculty of Chemistry, Northeast Normal University, Changchun, Jilin, 130024, P. R. China, and Faculty of Chemistry and Pharmacy, Jiamusi University, Jiamusi, HeilongJiang, 154007, P. R. China

Received December 12, 2007

Four new hybrids based on the Wells-Dawson polyoxometalate $[P_2W_{18}O_{62}]^{6-}$ (P_2W_{18}), $\{[Ag(bipy)]_2[P_2W_{18}O_{62}]\}\cdot 2[H_2bipy]\cdot 4H_2O$ (**1**), $\{[Ag(bipy)]_4[P_2W_{18}O_{62}]\}\cdot 2[Hbipy]$ (**2**), $K[P_2W_{18}O_{62}]\cdot 2.5[H_2bipy]\cdot 2H_2O$ (**3**), and $[P_2W_{18}O_{62}]_2\cdot [H_2bipy]_4\cdot [Hbipy]_4\cdot 3H_2O$ (**4**), were hydrothermally synthesized and structurally characterized by routine techniques and single-crystal X-ray diffraction. Compounds **1** and **2** are isolated at lower pH values. **1** represents a 3D (4,4)-net structure with NbO topology, in which the P_2W_{18} clusters are modified by four Ag−N coordination polymeric chains, and **2** exhibits a 3D (3,4)-net structure with the $(9^2\cdot 12)(8\cdot 10^4\cdot 12)(3^2\cdot 10^2\cdot 11^2)(3\cdot 6\cdot 10^2\cdot 12^2)$ topology, in which Ag-bipy layers are intercalated by the dimer of P_2W_{18} clusters in a staggering mode, and the P_2W_{18} clusters show the highest coordination number to date. By increasing the pH value, compounds **3** and **4** are obtained as supramolecular compounds. Their structural differences reveal that the pH value of the reaction system is the key factor influencing the structure and topology of these compounds, which can be explained by the acid−base chemistry of the molecular building units and silver chemistry.

Introduction

Explored early by Zubieta et al.[1] and You[2] et al., the design and synthesis of organic−inorganic hybrid materials based on polyoxometalates (POMs) through crystal engineering has become a significant research area today for POM chemists due to their versatile architectures[3] and potential applications in catalysis,[4] photochemistry,[5] electrochemistry,[6] magnetism,[7] and biochemistry.[8] As is well-known, POMs, as a large family of metal−oxygen clusters, have been viewed as ideal inorganic building blocks for the construction of multidimensional extended inorganic−organic hybrid materials, as they can not only provide a large number of terminal and bridging O atoms as multidentate inorganic ligands but also exhibit a wide variety of robust structural motifs with different sizes and topologies, ranging from closed cages and spherical shells to basket-, bowl-, barrel-, and belt-shaped structures.[3,9] Hence, the use of POMs as inorganic building blocks brews an appealing route to designing novel structural motifs with improved properties.

In recent years, by selecting the appropriate POMs as modular building blocks, many 1D, 2D, and 3D POM-based

* Author to whom correspondence should be addressed. E-mail: jpeng@nenu.edu.cn or pjun56@yahoo.com.
† Northeast Normal University.
‡ Jiamusi University.

(1) Hagrman, D.; Zubieta, C.; Rose, D. J.; Zubieta, J.; Haushalter, R. C. *Angew. Chem., Int. Ed. Engl.* **1997**, *36*, 873–875.
(2) Xu, Y.; Xu, J. Q.; Zhang, K. L.; Zhang, Y.; You, X. Z. *Chem. Commun* **2000**, *6*, 153–154.
(3) (a) Pope, M.T. *Heteropoly and Isopoly Oxometalates*; Springervelag: New York, 1983. (b) Pope, M. T.; Müller, A. *Polyoxometalate Chemistry from Topology via Self-Assembly to Applications*; Kluwer Academic Publishers: Dordrecht, The Netherlands, 2001.
(4) (a) Müller, A.; Pope, M. T.; Peters, F.; Gatteschi, D. *Chem. Rev.* **1998**, *98*, 239–272. (b) Artero, V.; Proust, A.; Herson, P.; Villain, F.; Moulin, C.; Gouzerh, P. *J. Am. Chem. Soc.* **2003**, *125*, 11156–11157.
(5) (a) Kögerler, P.; Cronin, L. *Angew. Chem., Int. Ed. Engl.* **2005**, *44*, 844–846. (b) Yamase, T. *J. Chem. Soc., Dalton Trans.* **1985**, *2585*, 2590.
(6) Coronado, E.; Galán-Mascarós, J. R.; Giménez-Saiz, C.; Gómez-García, C. J.; Martínez-Ferrero, E.; Almeida, M.; Lopes, E. B. *Adv. Mater.* **2004**, *16*, 324–327.
(7) (a) Pope, M. T.; Müller, A. *Angew. Chem., Int. Ed. Engl.* **1991**, *30*, 34–48. (b) Müller, A. *Nature.* **1991**, *352*, 115–115. (c) Coronado, E.; Gómez-García, C. J. *Chem. Rev.* **1998**, *98*, 273–296. (d) Lisnard, L.; Mialane, P.; Dolbecq, A.; Marrot, J.; Clemente-Juan, J. M.; Coronado, E.; Keita, B.; Oliveira, P.; Nadjo, L.; Secheresse, F. *Chem.—Eur. J.* **2007**, *13*, 3525–3536.
(8) (a) Rhule, J. T.; Hill, C. L.; Judd, D. A. *Chem. Rev.* **1998**, *98*, 327–358. (b) Wang, X.; Liu, J.; Pope, M. *Dalton Trans.* **2003**, *957*, 960.

10.1021/ic702407y CCC: $40.75
Published on Web 05/16/2008

hybrids have been successfully synthesized by Zubieta,[10] Pope,[11] Wang,[12] Wei,[13] Cronin,[14] and their respective co-workers. In this field, compared with other classical POMs, such as Keggin-, Anderson-, and Lindqvist-type anions, the hybrid materials based on the Wells-Dawson-type POMs are much less common, maybe due to their larger steric hindrance. Since the first example of a 1D Wells-Dawson hybrid was reported by the Yan group,[15] a series of 0D and 1D hybrids based on Wells-Dawson POMs and transition metal complexes (TMCs) have been reported.[16] And very recently, the first 2D example, $(NH_4)_3(4,4'\text{-}H_2bipy)[Cu(4,4'\text{-}bipy)]_7[P_2W_{18}O_{62}]_2\cdot 10H_2O$, was reported by the Wang group.[17] But only one 3D derivative based on the Wells-Dawson POMs has been reported by us hitherto.[18] So the construction of TMC-modified Wells-Dawson POMs is a challenging issue. Note that, although there is larger steric hindrance with the Wells-Dawson POMs, their 54 coordination O atoms (18 terminal and 36 μ_2-O atoms) offer many smart potential sites to link more TMC units, and two categories of metal atoms (6 polar and 12 equatorial metal atoms) make the steric orientations of the coordination sites more flexible, which may decrease the hindrance of coordinated TMCs and make the covalent grafting of POMs easier. Both are positive aspects for the modifying chemistry of the Wells-Dawson POMs. To extend this field, several factors must be taken into account: the coordination nature of metal ions, the steric hindrance of the ligands, and the geometrical relations between the POMs and the TMCs.

Additionally, some 3D TMC-modified POMs[19] give us the hint that the soft d^{10} metal ions and the rigid 4,4′-bipy molecules are good candidates for the construction of the 3D TMC-modified POMs with high connectivity. First, the soft d^{10} metal ions adopt versatile coordination geometries under hydrothermal conditions, especially the Ag^+ ions, which can display geometries of two to seven coordination bonds, such as linear, T-type, "seesaw", "square-pyramidal", and "trigonal-bipyramidal" geometries, and so on.[20] Second, 4,4′-bipy is a rodlike molecule and is commonly used as a bridging bidentate ligand with small steric hindrance. Finally, the TMCs constructed by Ag^+ ions and 4,4′-bipy molecules possess coordination freedom, allowing them to conform the coordination environment of the POMs.

Although the hydrothermal technique has been extensively used to create novel structures, from the crystal engineering point of view, the control of self-assembly processes is still a very challenging work for realizing the target syntheses of the inorganic−organic hybrid materials based on POMs. Many parameters such as initial reactants and their stoichiometry, pH value, crystallization temperature, and pressure can significantly affect the topological structures. To address the effect of these factors on the construction of hybrids, many efforts have been made. For example, Long's group and our group have discussed the influences of steric hindrance of the organic ligands, the POM anions, and the pH values on the structures of POM-based hybrids;[19,21] Zubieta and co-workers and our group have also discussed the influence of metal ions on the structure of POM-based hybrids.[10,19] However, it would take more examples to rationalize the results.

On the basis of the aforementioned points, we have chosen Wells-Dawson POMs and Ag^+/4,4′-bipy TMCs as building blocks to construct the high-dimensional and high-connected POM-based hybrids in this work. During the research, we found that the pH value was a crucial factor for final product determination. We therefore systematically investigated the effect of pH value on the assembly of the POM-based hybrid materials. Herein, we reported hydrothermal synthesis under different pH conditions and the crystal structures of $\{[Ag(bipy)]_2[P_2W_{18}O_{62}]\}\cdot 2[H_2bipy]\cdot 4H_2O$ (**1**), $\{[Ag(bipy)]_4$-

(9) (a) Wang, E. B.; Hu, C. W.; Xu, L. *Introduction of Polyoxometalate Chemistry*; Chemistry Industry Press: Beijing, 1997. (b) Gouzerh, P.; Proust, A. *Chem. Rev.* **1998**, *98*, 77–112. (c) Hill, C. L. *Chem. Rev.* **1998**, *98*, 1–2.

(10) (a) Soghomonian, V.; Chen, Q.; Haushalter, R. C.; Zubieta, J.; O'Connor, J. C. J.; Leelc, Y. S. *Chem. Mater.* **1993**, *5*, 1690–1691. (b) LaDuca, R. L., Jr.; Rarig, R. S., Jr.; Zubieta, J. *Inorg. Chem.* **2001**, *40*, 607–612. (c) Hagrman, P. J.; Zubieta, J. *Inorg. Chem.* **2001**, *40*, 2800–2809. (d) Pamela, Z. J.; Robert, L., Jr.; Randy, S. R., Jr.; Kenneth, M. J.; Zubieta, J. *Inorg. Chem.* **1998**, *37*, 3411–3414. (e) Hagrman, P. J.; LaDuca, R. L., Jr.; Koo, H. J.; Rarig, R., Jr.; Haushalter, R. C.; Whangbo, M. H.; Zubieta, J. *Inorg. Chem.* **2000**, *39*, 4311–4317. (f) Hagrman, P. J.; Zubieta, J. *Inorg. Chem.* **2000**, *39*, 5218–5224.

(11) (a) Masahiro, S.; Dickman, M. H.; Pope, M. T. *Angew. Chem., Int. Ed.* **2000**, *39*, 2914–2916. (b) Mbomekalle, I. M.; Keita, B.; Lu, Y. W.; Nadjo, L.; Contant, R.; Belai, N.; Pope, M. T. *Eur. J. Inorg. Chem.* **2004**, *276*, 285. (c) Wei, X. Y.; Dickman, M. H.; Pope, M. T. *J. Am. Chem. Soc.* **1998**, *120*, 10254–10255.

(12) (a) Wang, X. L.; Qin, C.; Wang, E. B.; Su, Z. M.; Li, Y. G.; Xu, L. *Angew. Chem., Int. Ed.* **2006**, *45*, 7411–7414. (b) An, H. Y.; Xiao, D. R.; Wang, E. B.; Li, Y. G.; Su, Z. M.; Xu, L. *Angew. Chem. Int. Ed.* **2006**, *45*, 904–908. (c) Jin, H.; Qi, Y. F.; Wang, E. B.; Li, Y. G.; Qin, C.; Wang, X. L.; Chang, S. *Eur. J. Inorg. Chem.* **2006**, *22*, 4541. (d) Qi, Y. F.; Li, Y. G.; Qin, C.; Wang, E. B.; Jin, H.; Xiao, D. R.; Wang, X. L.; Chang, S. *Inorg. Chem.* **2007**, *46*, 3217–3230.

(13) (a) Wu, P. F.; Li, Q.; Ge, N.; Wei, Y. G.; Wang, Y.; Wang, P.; Guo, H. Y. *Eur. J. Inorg. Chem.* **2004**, *2819*, 2822. (b) Wei, Y. G.; Xu, B. B.; Barnes, C. L.; Peng, Z. H. *J. Am. Chem. Soc.* **2001**, *123*, 4083–4084. (c) Li, Q.; Wei, Y. G.; Hao, J.; Zhu, Y. L.; Wang, L. S. *J. Am. Chem. Soc.* **2007**, *129*, 5810–5811.

(14) (a) Akutagawa, T.; Endo, D.; Imai, H.; Noro, S. I.; Cronin, L.; Nakamura, T. *Inorg. Chem.* **2006**, *45*, 8628–8637. (b) Streb, C.; Ritchie, C.; Long, D. L.; Kögerler, P.; Cronin, L. *Angew. Chem., Int. Ed.* **2007**, *46*, 7579–7582. (c) Abbas, H.; Pickering, A. L.; Long, D. L.; Cronin, L. *Chem.—Eur. J.* **2005**, *11*, 1071–1078. (d) Long, D. L.; Kögerler, P.; Cronin, L. *Angew. Chem., Int. Ed.* **2004**, *43*, 1817–1820. (e) Long, D. L.; Kögerler, P.; Farrugia, L. J.; Cronin, L. *Angew. Chem., Int. Ed.* **2003**, *42*, 4180–4183.

(15) Yan, B. B.; Xu, Y.; Bu, X. H.; Goh, N. K.; Chia, L. S.; Stucky, G. D. *J. Chem. Soc., Dalton Trans.* **2001**, *13*, 2009–2014.

(16) (a) Soumahoro, T.; Burkholder, E.; Ouellette, W.; Zubieta, J. *Inorg. Chem. Acta* **2005**, *358*, 606–616. (b) Tian, A. X.; Han, Z. G. ; Peng, J.; Dong, B. X.; Sha, J. Q.; Li, B. *J. Mol. Struct.* **2007**, *832*, 117–123.

(17) Jin, H.; Qi, Y. F.; Xiao, D. R.; Wang, X. L.; Chang, S.; Wang, E. B. *J. Mol. Struct.* **2007**, *837*, 23–29.

(18) Sha, J. Q.; Wang, C.; Peng, J.; Chen, J.; Tian, A. X.; Zhang, P. P. *Inorg. Chem. Commun.* **2007**, *10*, 1321–1324.

(19) (a) Dong, B. X.; Peng, J.; Gomez-Garcia, C. J.; Benmansour, S.; Jia, H. Q.; Hu, N. H. *Inorg. Chem.* **2007**, *46*, 5933–5941. (b) Sha, J. Q.; Peng, J.; Liu, H. S.; Chen, J.; Tian, A. X.; Zhang, P. P. *Inorg. Chem.* **2007**, *46*, 11183–11189. (c) Sha, J. Q.; Peng, J.; Liu, H. S.; Xue, B.; Chen, J.; Tian, A. X.; Dong, B. X.; Zhang, P. P. *J. Mol. Struct.* **2007**, 85–91.

(20) (a) Pickering, A. L.; Long, D. L.; Cronin, L. *Inorg. Chem.* **2004**, *43*, 4953–4961. (b) Villanneau, R.; Proust, A.; Robert, F.; Gouzerh, P. *Chem. Commun.* **1998**, *1491*, 1492.

(21) (a) Ren, Y. P.; Kong, X. J.; Hu, X. Y.; Sun, M.; Long, L. S. *Inorg. Chem.* **2006**, *45*, 4016–4024. (b) Ren, Y. P.; Kong, X. J.; Long, L. S.; Huang, R. B.; Zheng, L. S. *Cryst. Growth Des.* **2006**, *6*, 572–576. (c) Kong, X. J.; Ren, Y. P.; Zheng, P. Q.; Long, Y. X.; Long, L. S.; Huang, R. B.; Zheng, L. S. *Inorg. Chem.* **2006**, *45*, 10702–10711. (d) Zheng, P. Q.; Ren, Y. P.; Long, L. S.; Huang, R. B.; Zheng, L. S. *Inorg. Chem.* **2005**, *44*, 1190–1192.

Scheme 1. Schematic Illustration of the Synthesis Routes of **1**−**4**

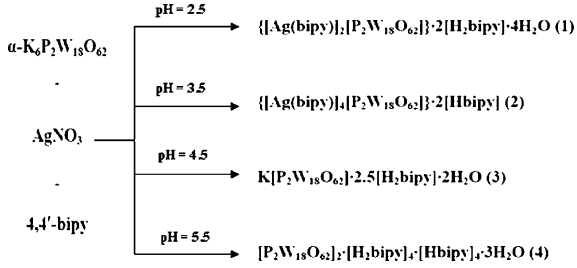

$[P_2W_{18}O_{62}]\}\cdot 2[Hbipy]$ (**2**), $K[P_2W_{18}O_{62}]\cdot 2.5[H_2bipy]\cdot 2H_2O$ (**3**), and $[P_2W_{18}O_{62}]_2\cdot[H_2bipy]_4\cdot[Hbipy]_4\cdot 3H_2O$ (**4**), which showed that the pH value of the reaction system played a key role in the structural control of the self-assembled process (Scheme 1).

Experimental Section

Materials and Methods. All reagents were purchased commercially and used without further purification. α-$K_6P_2W_{18}O_{62}\cdot 15H_2O$ was prepared according to the literature method[22] and verified by the IR spectrum. Elemental analyses (C, H, and N) were performed on a Perkin- Elmer 2400 CHN Elemental Analyzer. The IR spectra were obtained on an Alpha Centaurt FT/IR spectrometer with KBr pellets in the 400−4000 cm^{-1} region. The thermogravimetric (TG) analyses were carried out on a Perkin-Elmer TGA7 instrument in flowing N_2 with a heating rate of 10 °C/min. Cyclic voltammograms were obtained with a CHI 660 electrochemical workstation at room temperature. Platinum gauze was used as a counter electrode, and a Ag/AgCl electrode was referenced. Chemically bulk-modified carbon paste electrodes (CPEs) were used as working electrodes.

Syntheses. $\{[Ag(bipy)]_2[P_2W_{18}O_{62}]\}\cdot 2[H_2bipy]\cdot 4H_2O$ (1). A mixture of α-$K_6P_2W_{18}O_{62}\cdot 15H_2O$ (0.1 mmol, 490 mg), 4,4′-bipy (0.2 mmol, 40 mg), $AgNO_3$ (0.4 mmol, 68 mg), NH_4VO_3 (0.1 mmol, 12 mg), and triethylamine (0.1mmol) was dissolved in 10 mL of distilled water at room temperature. When the pH value of the mixture was adjusted to about 2.5 with a 1.0 M HCl solution, the suspension was put into a Teflon-lined autoclave and kept under autogenous pressure at 160 °C for 6 days. After slow cooling to room temperature, yellow shield crystals of **1** were filtered and washed with distilled water (39% yield based on W). Anal. calcd for $C_{40}H_{44}N_8Ag_2O_{66}P_2W_{18}$ (5279.8): C, 9.09; H, 0.83; N, 2.12. Found: C, 9.03; H, 0.87; N, 2.08. IR (solid KBr pellet/cm^{-1}): 3415(s), 3092(w), 1607(m), 1533(m), 1482(w), 1415(m), 1312(w), 1218(m), 1087(s), 950(s), 898(m), 766(s), 520(m).

$\{[Ag(bipy)]_4[P_2W_{18}O_{62}]\}\cdot 2[Hbipy]$ (2). The synthetic method, here was similar to that used for the preparation of **1**, except that the pH value was adjusted to 3.5. Yellow polyhedron crystals suitable for X-ray analyses were obtained in 38% yield based on W. Anal. calcd for $C_{60}H_{50}N_{12}Ag_4O_{62}P_2W_{18}$ (5733.82): C, 12.56; H, 0.87; N, 2.93. Found: C, 12.53; H, 0.91; N, 2.89. IR (solid KBr pellet/cm^{-1}): 3444(s), 3073(w), 1606(m), 1502(m), 1474(w), 1415(m), 1322(w), 1214(m), 1085(s), 945(s), 901(m), 765(s), 524(m).

$K[P_2W_{18}O_{62}]\cdot 2.5[H_2bipy]\cdot 2H_2O$ (3). Compound **3** was prepared in a manner similar to that described for **1**, except that the pH value was adjusted to 4.5. Black bar crystals suitable for X-ray analysis were obtained in 34% yield based on W. Anal. calcd for $C_{25}H_{29}N_5KO_{64}P_2W_{18}$ (4833.81): C, 6.21; H, 0.60; N, 1.45. Found: C, 6.22; H, 0.66; N, 1.44. IR (solid KBr pellet/cm^{-1}): 3437(s), 3079(w), 1604(m), 1488(m), 1406(m), 1362(w), 1238(m), 1202(m), 1085(s), 948(s), 904(m), 765(s), 521(m).

$[P_2W_{18}O_{62}]_2\cdot[H_2bipy]_4\cdot[Hbipy]_4\cdot 3H_2O$ (4). Compound **4** was prepared in a manner similar to that described for **1**, except that the pH value was adjusted to 5.5. Black block crystals suitable for X-ray analysis were obtained in 42% yield based on W. Anal. calcd for $C_{80}H_{82}N_{16}O_{127}P_4W_{36}$ (10042): C, 9.56; H, 0.82; N, 2.23. Found: C, 9.53; H, 0.88; N, 2.19. IR (solid KBr pellet/cm^{-1}): 3437(s), 3079(w), 1610(m), 1490(m), 1410(m), 1336(w), 1215(m), 1085(s), 947(s), 901(m), 777(s), 520(m).

Preparations of 1-, 2-, 3-, 4-CPEs. The compound **1** modified carbon paste electrode (**1**-CPE) was fabricated as follows: 48 mg of graphite powder and 8 mg of **1** were mixed and ground together by agate mortar and pestle to achieve a uniform mixture, and then 0.6 mL of nujol was added with stirring. The homogenized mixture was packed into a glass tube with a 1.2 mm inner diameter, and the tube surface was wiped with paper. Electrical contact was established with a copper rod through the back of the electrode. In a similar manner, **2**-, **3**-, **4**-CPEs were made with **2**, **3**, and **4**.

X-Ray Crystallographic Study. Crystal data for compounds **1**−**4** were collected on a Bruker SMART-CCD diffractometer, with Mo Kα monochromatic radiation (λ = 0.710 73 Å) at 293 K. All structures were solved by direct methods and refined by full-matrix least-squares on F^2 using the *SHELXTL* crystallographic software package.[23] Some of non-hydrogen atoms were refined isotropically in compounds because of the large unit cell volumes and relatively weak average intensities. For the compounds, all of the hydrogen atoms on carbon atoms were generated geometrically, while the hydrogen atoms attached to water molecules were not located but were included in the structure factor calculations. The crystal data and structure refinements of compounds **1**−**4** are summarized in Table 1. Selected bond lengths and angles for compounds **1**−**4** are listed in Table S1−S4 (Supporting Information).

Results and Discussion

The α-$[P_2W_{18}O_{62}]^{6-}$ (abbreviated to P_2W_{18}) anion is the inorganic building block in compounds **1**−**4**, which contains two $[\alpha$-A-$PW_9O_{34}]^{9-}$ units derived from an α-Keggin anion by removal of a set of three corner-shared WO_6 octahedra. The P−O and W−O lengths are in the normal ranges.[24] Bond valence sum calculations show that all tungsten atoms are in +VI oxidation states, and silver atoms are in +I oxidation states.

Structure Description of Compound 1. Single-crystal X-ray diffraction analysis reveals that **1** is a three-dimensional (3D) compound with NbO topology. As shown in Figure 1, left, there is one polyoxoanion $[P_2W_{18}O_{62}]^{6-}$, two $[Ag(4,4'\text{-bipy})]^+$ cations, two discrete bipy molecules, and four water molecules of crystallization. Each P_2W_{18} cluster acts as tetra-dentate inorganic ligand coordinating to four silver centers (shown in Figure 1, right).

In compound **1**, there is a crystallographically independent silver atom, which adopts a tetra-coordinated seesaw-shaped

(22) Lyon, D. K.; Miller, W. K.; Novet, T.; Domaille, P. J.; Evitt, E.; Johnson, D. C.; Finke, R. G. *J. Am. Chem. Soc.* **1991**, *113*, 7209–7221.

(23) (a) Sheldrick, G. M. *SHELXS-97, Program for Crystal Structure Solution*; University of Göttingen: Göttingen, Germany, 1997. (b) Sheldrick, G. M. *SHELXL-97, Program for Crystal Structure Refinement*; University of Göttingen: Göttingen, Germany, 1997.

(24) (a) Wang, J. P.; Zhao, J. W.; Niu, J. Y. *J. Mol. Struct.* **2004**, *697*, 191–198. (b) Lu, Y.; Xu, Y.; Li, Y. G.; Wang, E. B.; Xu, X. X.; Ma, Y. *Inorg. Chem.* **2006**, *45*, 2055–2060.

Table 1. Crystal Data and Structure Refinements for Compounds **1**−**4**

	1	**2**	**3**	**4**
chemical formula	$C_{40}H_{44}N_8Ag_2O_{66}P_2W_{18}$	$C_{60}H_{50}N_{12}Ag_4O_{62}P_2W_{18}$	$C_{25}H_{29}N_5KO_{64}P_2W_{18}$	$C_{80}H_{82}N_{16}O_{127}P_4W_{36}$
CCDC	657231	657232	657233	657234
M_r	5279.8	5733.82	4833.81	10042
cryst syst	orthorhombic	orthorhombic	triclinic	triclinic
space group	*Cmma*	*Pccn*	$P\bar{1}$	$P\bar{1}$
a/Å	19.9227(8)	49.793(5)	13.394(3)	13.9593
b/Å	21.9105(8)	17.495(5)	14.177(3)	16.3813
c/Å	22.6668(9)	22.705(5)	26.955(5)	20.8524
α/deg	90	90	78.04(3)	83.753
β/deg	90	90	83.03(3)	72.603
γ/deg	90	90	67.66(3)	67.054
V/Å^3	9894.4(7)	19779(7)	4626.4(16)	4190.02
T/K	273(2)	293(2)	293(2)	296 (2)
Z	4	8	2	1
D_c/mg cm^{-3}	4.051	3.341	2.446	4.058
μ(Mo Kα)/mm^{-1}	21.329	1.452	3.513	24.739
θ range (deg)	0.9−28.32	0.82−26.31	3.03−25.00	1.65−25.00
total reflns	30549	105558	36356	21237
ind. reflns	6476	20023	16164	14558
R_{int}	0.0619	0.1361	0.0975	0.0411
R_1[a] [$I > 2\sigma(I)$]	0.0539	0.0713	0.0686	0.0866
wR_2[b] [$I > 2\sigma(I)$]	0.1778	0.1789	0.1808	0.2370

[a] $R_1 = \sum||F_o| - |F_c||/\sum|F_o|$. [b] $wR_2 = \sum\{[w(F_o^2 - F_c^2)^2]/\sum[w(F_o^2)^2]\}^{1/2}$.

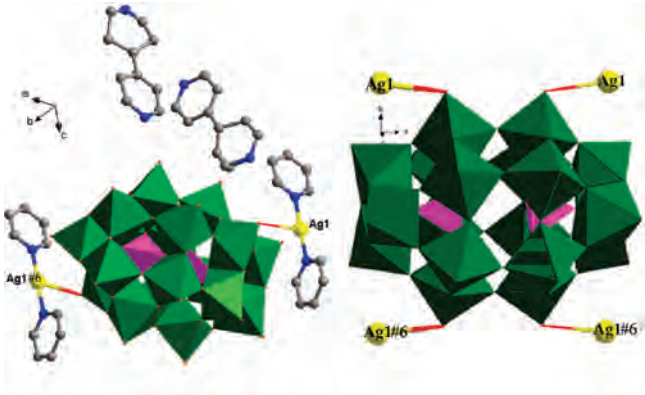

Figure 1. Left: Combined polyhedral and ball/stick representation of the molecular structure unit of **1**. All of the hydrogen atoms and water molecules have been omitted for clarity. Right: The view of coordination details of P_2W_{18} clusters (#6 $-x + 1/2$, $y + 1/2$, z).

geometry achieved by two N atoms of two 4,4′-bipy and two O atoms of two P_2W_{18} clusters. The bond distances around the Ag(I) ions are 2.134−2.138 Å (Ag1−N) and 2.841 Å (Ag1−O), the N−Ag−N angle is 180°, and the O−Ag−O angle is 169.89°. In the framework, Ag ions connect the POMs and bipy molecules into a 3D architecture, which can be considered being constructed from two moieties.

One moiety is the 2D layer formed by P_2W_{18} clusters and silver atoms. In the 2D layer, each Ag atom covalently links to two adjacent P_2W_{18} clusters via Ag−O bonds, and each P_2W_{18} cluster provides four terminal oxygen atoms linking with four Ag atoms, shown in Figure 2 (left). The other moiety is an array of infinite $[Ag(bipy)]_n^{n+}$ chains, shown in Figure 2 (right). The two moieties are fused together by the Ag^+ ions, resulting in a 3D framework, as shown in Figure 3a (left), in which each P_2W_{18} cluster is modified by four $[Ag(bipy)]_n^{n+}$ chains like four tracks. A fascinating structural feature is that compound **1** is a NbO topology hybrid based on POMs with the topology symbol $(6^4\cdot8^2)(6^4\cdot8^2)$, when P_2W_{18} clusters and Ag atoms are taken as four-connected nodes, shown in Figure 3a (right).

Structure Description of Compound 2. Single-crystal X-ray diffraction analysis shows that compound **2** is also a 3D framework with $(9^2\cdot12)(8\cdot10^4\cdot12)(3^2\cdot10^2\cdot11^2)(3\cdot6\cdot10^2\cdot12^2)$ topology. As shown in Figure 4 (left), there is one polyoxoanion $[P_2W_{18}O_{62}]^{6-}$, four $[Ag(4,4'\text{-bipy})]^+$ cations, and two discrete bipy molecules. There are three noticeable features. First, the P_2W_{18} clusters act as penta-dentate inorganic ligands coordinating to seven silver centers, shown in Figure 4 (right). Although the Wells-Dawson-type anion has abundant oxygen atoms available to coordinate to TMCs, its connection number reported was no more than four. So compound **2** represents the highest connection number to date. Second, the POMs exhibit various coordination fashions, including terminal, bridging, and chelate styles, and the coexistence of the multiple coordination fashions makes the modification of the Wells-Dawson POMs with more TMCs easier. The various coordination modes have never been reported to date. Finally, Ag atoms also represent multiple coordination geometries. There are four crystallographically independent silver atoms (Ag1, Ag2, Ag3, and Ag4), which exhibit three sorts of coordination geometries coexisting in the structure, namely, three-coordinated "T-shaped" geometry of $\{Ag(3)N_2O\}$ by two N atoms of bipy ligands and one O atom of one P_2W_{18} cluster, four-coordinated "seesaw" geometry of $\{Ag(1,4)N_2O_2\}$ coordinated by two N atoms of two bipy ligands and two O atoms of two P_2W_{18} clusters, and five-coordinated square-pyramidal geometry ($\tau = (\beta - \alpha)/60 = 0.18$)[25] of $\{Ag(2)N_2O_3\}$ coordinated by two N atoms of two bipy ligands and three O atoms of two P_2W_{18} clusters. The bond distances around the Ag ions are 2.134−2.138Å (Ag−N) and 2.552−2.828 Å (Ag−O), while the N−Ag−N angles are 164.9−175.9° and O−Ag−O angles are 148.7−152.6°. To the best of our

(25) Addison, A. W.; Rao, T. N. *J. Chem. Soc., Dalton Trans.* **1984**, *1349*, 1356.

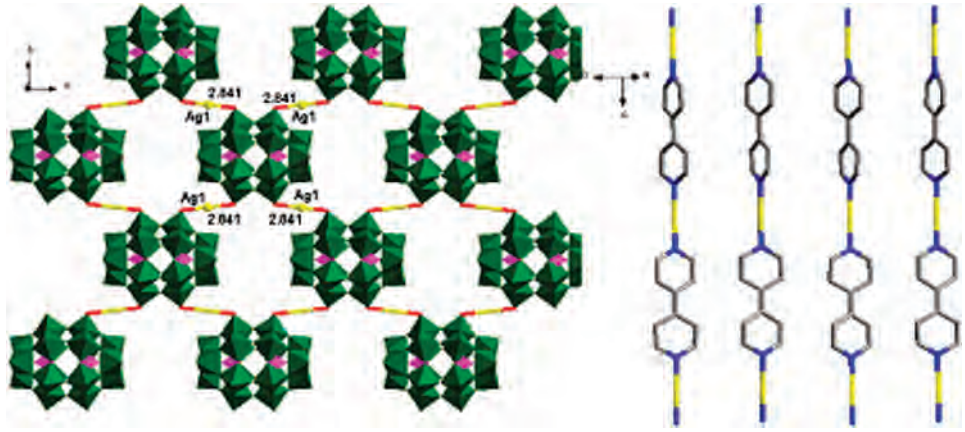

Figure 2. Left: Polyhedral and ball/stick representation of the 2D layer of **1**. All of the hydrogen atoms and water molecules have been omitted for clarity (the yellow balls symbolize Ag atoms). Right: Stick representation of $[Ag(bipy)]_n^{n+}$ chains.

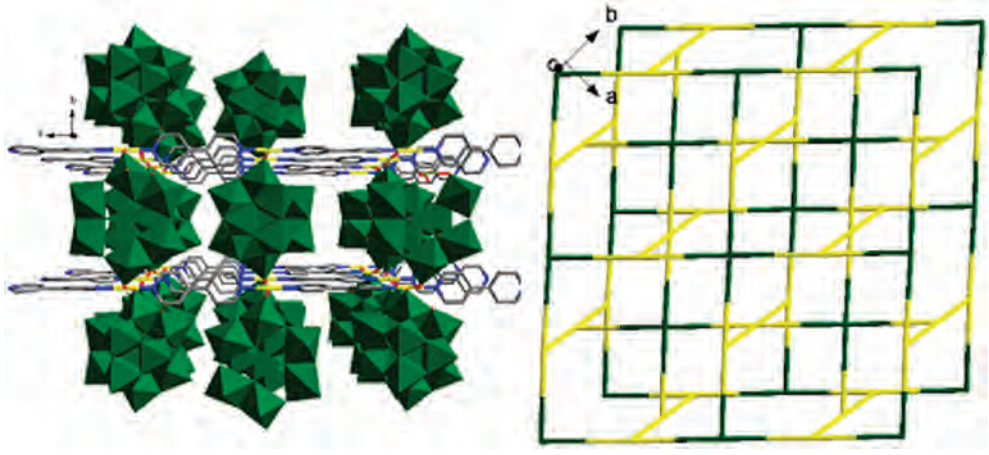

Figure 3. (a) Combined polyhedral/stick representation of a 3D structure in **1**. (b) View of the topology of compound **1** (the green nodes symbolize the P_2W_{18} clusters, and the yellow nodes symbolize Ag atoms).

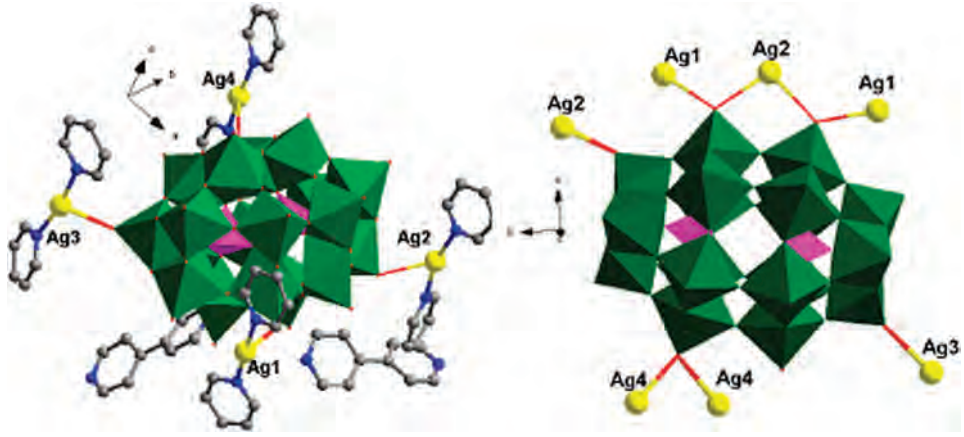

Figure 4. Left: Combined polyhedral and ball/stick representation of the molecular structure unit of **2**. All of the hydrogen atoms and water molecules have been omitted for clarity. Right: The coordination view of the P_2W_{18} cluster.

knowledge, these different coordination modes and configurations of Ag^+ ions coexisting in one compound have not been found in the other POMs. The phenomenon is also in favor of the forming of high-connectivity Wells-Dawson POMs. In summary, the coordination number and the fashion of the POMs and the coordination modes of Ag^+ ions together lead to the formation of high-connected Wells-Dawon POMs (shown in Scheme 2), which testifies to our synthetic strategy.

Similar to compound **1**, the structure of **2** is also constructed by the 2D layer formed by the P_2W_{18} clusters and silver atoms (shown in Figure 5) and the array of infinite $[Ag(bipy)]_n^{n+}$ chains. The two moieties are fused together by the Ag ions, resulting in a 3D framework. But, different from **1**, on one hand, in the P_2W_{18}/Ag layer, the POMs are dimerized by double Ag bridges, and Ag atoms are linked together into a −O−Ag−O− chain *via* Ag−O bonds. On the other hand, the array of infinite $[Ag(bipy)]_n^{n+}$ chains also

Scheme 2. Schematic Illumination of Combination of the Three Features in the Structure of High-Connected Wells-Dawson POMs[a]

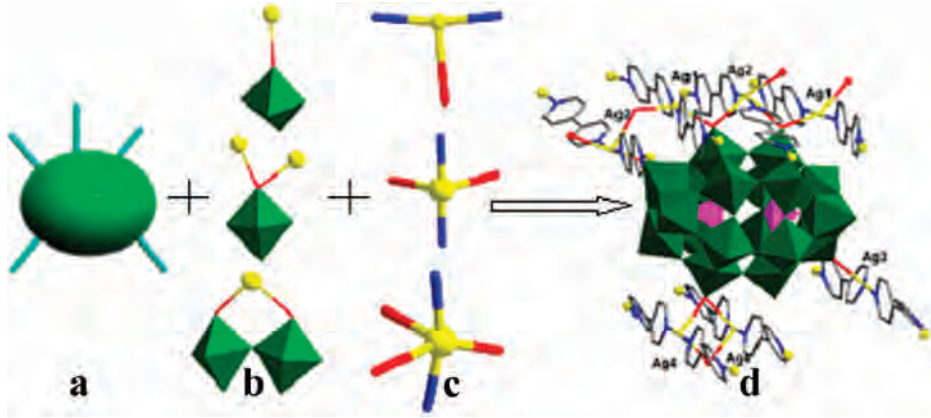

[a] **a** represents the coordination number of the POMs. **b** represents the fashion of the POMs. **c** represents the coordination modes of Ag^+ ions, and **d** represents the high-connected Wells-Dawson POMs due to the aggregation of the three factors (**a**, **b**, and **c**).

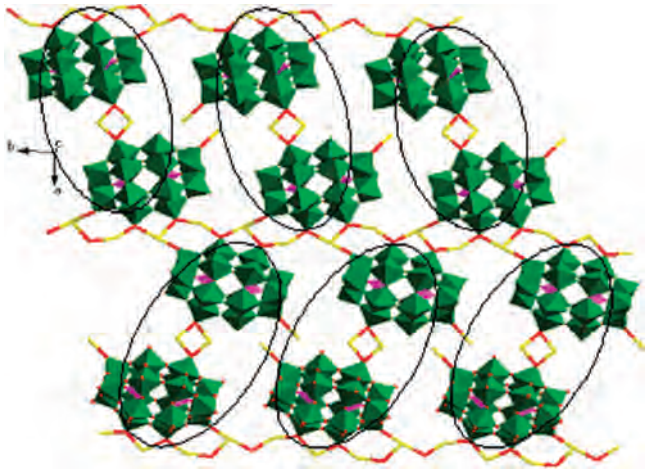

Figure 5. Polyhedral/stick representation of the 2D structure of **2** constructed by POMs and Ag ions.

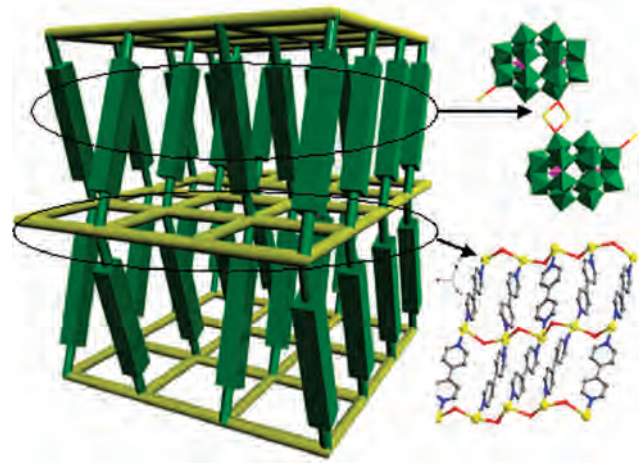

Figure 6. The 3D schematic illustrations of **2**. The inset shows a plot of the polyhedral and stick representation of the dimer of P_2W_{18} clusters (top) and the ball/stick representation of Ag-bipy layers (below).

exhibits two interesting features: one is the formation of the double $[Ag(bipy)]_n^{n+}$ chains due to the binding of the bipy molecules to the double Ag bridges (shown in Figure S1, Supporting Information); the other is that the infinite $[Ag(bipy)]_n^{n+}$ chains are linked into Ag−bipy layers *via* O bridges (shown in the inset of Figure 6). If the double $[Ag(bipy)]_n^{n+}$ chains are omitted, the 3D framework can be viewed as the Ag−bipy layers intercalated by the dimer of P_2W_{18} clusters in a staggering mode, shown in Figure 6.

Furthermore, the 3D structure can be rationalized as a (3,4) connecting network with $(9^2\cdot12)(8\cdot10^4\cdot12)(3^2\cdot10^2\cdot11^2)$-$(3\cdot6\cdot10^2\cdot12^2)$ topology, if we assign −Ag−bipy−Ag− and −O−Ag−O− as the connectors and the P_2W_{18} clusters and Ag atoms as the nodes. In this simplification, Ag3 atoms are the three-connected nodes, and Ag1/Ag2 and Ag4 atoms are the four-connected ones. To the best of our knowledge, this topology framework has never been observed in POM chemistry. It should be also emphasized that compound **2** is the first self-penetrating network containing Wells-Dawson POMs, shown in inset of Figure 7.

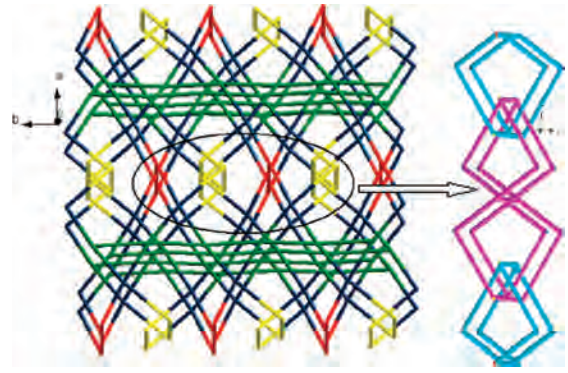

Figure 7. View of the topology of compound **2** (the blue nodes symbolize the P_2W_{18} clusters, the yellow nodes symbolize Ag3 atoms, the green nodes symbolize Ag4 atoms, and the red nodes symbolize Ag1/Ag2 atoms). The inset shows the plot of a self-penetrating network.

Structure Description of Compounds 3 and 4. Single-crystal X-ray diffraction analyses show that compounds **3** and **4** consist of one Wells-Dawson polyoxoanion, bipy molecules (three for **3** and four for **4**), one K^+ ion (only for **3**), and water molecules (shown in Figure 8). There is a linear $(bipy)_4$ fragment with distances of 2.553 Å for N2···N2 and 2.609 Å for N3···N4 (shown in Figure 9, top). These short separations indicate that the bipy molecules are protonized and H-bonding interactions exist between them. The Wells-Dawson anions are linked together by the linear tetrad $(bipy)_4$, forming a 2D supramolecular layer via the weak

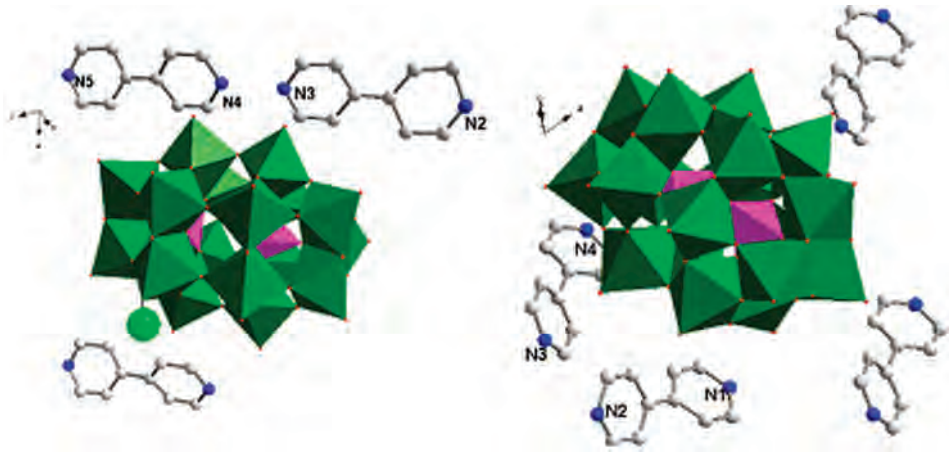

Figure 8. Combined polyhedral and ball/stick representation of the molecular structure unit of **3** (left) and **4** (right).

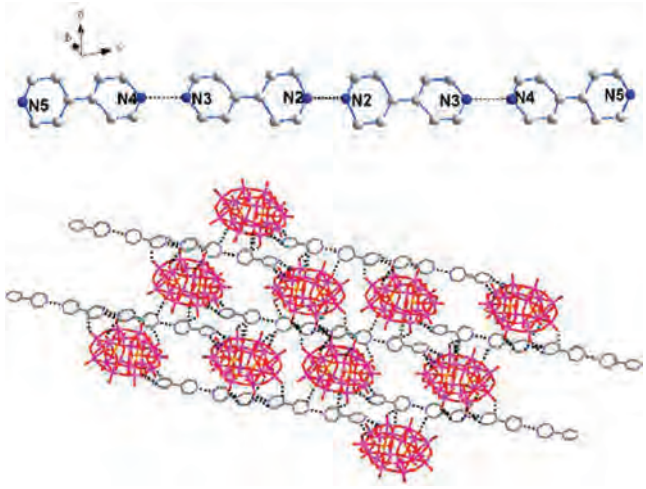

Figure 9. Top: The ball/stick representation of the linear tetrad $(bipy)_4$ framework. Bottom: Supramolecular framework structure of hydrogen-bonding linkage for compound **3**. All hydrogen atoms are omitted.

interactions (shown in Figure 9, bottom). Furthermore, the 2D layers are linked by other bipy molecules to form a 3D supramolecular structure (shown in Figure S2, Supporting Information). Compound 4 also exhibits a 3D supramolecular network structure based on weak interactions with the shortest N···N distance being 2.726 Å (shown in Figure S3, Supporting Information).

Influence of the pH Value on the Structures of Compounds 1−4. Compounds **1**−**4** were synthesized under the same reaction conditions, except for the alternation of one pH unit. It is clear that the pH value of the reaction system is the key factor influencing the structures and topologies of these compounds, which indicates that the assembly process is pH-dependent. At lower pH values, compounds **1** and **2** are isolated. Let us recall that the POMs in **1** are modified by four Ag−bipy chains and in **2** by seven Ag−bipy chains; with an increase of the pH value, supramolecular polymers based on Wells-Dawson POMs are formed (**3** and **4**). A similar effect has been observed in other organic−inorganic hybrids based on Keggin POMs.[21d] The structural differences of **1**−**4** can be reasonably explained by the acid−base chemistry of the molecular building units and silver chemistry.

First, because the free Ag^+ ions are readily transformed to Ag or Ag_2O under hydrothermal conditions, the change of Ag source during the reaction must be taken into account. At the lower pH values, the Ag^+ ions, without hydrolysis, are sufficient for the coordination of the bipy molecules and POM, which results in the fact that the P_2W_{18} cluster is modified by four parallel $[Ag(bipy)]_n^{n+}$ chains in **1** and seven parallel $[Ag(bipy)]_n^{n+}$ chains in **2.**

With the pH value continuously increasing, free Ag^+ ions decrease greatly, so that the protonization of bipy is more favorable than the coordination of bipy to Ag^+. This results in the disappearace of Ag^+ ions in compounds **3** and **4**. Finally, the extent of protonization of bipy becomes a little weaker as the pH increases by 1 from pH 4.5 in **3** to pH 5.5 in **4**, as proven by the ratio of H^+ to bipy of 2 in **3** and 1.5 in **4**.

FT-IR Spectra, TG Analyses. The IR spectra of compounds **1**−**4** (Figure S4a−d, Supporting Information) are similar: four characteristic peaks of POMs at 1085−1087 cm^{-1} ascribed to $\upsilon(P-O_a)$, 944−950 cm^{-1} ascribed to $\upsilon(W-O_t)$, 898−904 cm^{-1} ascribed to $\upsilon(W-O_b-W)$, and 765−777 cm^{-1} ascribed to $\upsilon(W-O_c-W)$ (where O_t = terminal oxygen, O_b = bridged oxygen of two octahedra sharing a corner, and O_c = bridged oxygen of two octahedra sharing an edge). The characteristic bands in the region from 1410 to 1640 cm^{-1} can be regarded as features of the 4,4′-bipy group.

The thermal stabilities of compounds **1**−**4** were investigated under a N_2 atmosphere from 40 to 800 °C, and the TG curves are provided in Figure S5 (Supporting Information). For compound **1**, the weight loss of 1.44% (calcd 1.36%) below 190 °C was attributed to the release of the crystal water molecules. According to the differential thermal analysis curve, the anhydrous compound began to decompose at 345 °C. In the range of 345−650 °C, the weight loss of 15.16% was assigned to the decomposition of bipy ligands and POMs. The whole weight loss (16.60%) is in good agreement with the calculated value (16.55%). The anhydrous compound, **2**, was stable up to 350 °C. Upon further heating, weight loss was caused by the decomposition of bipy ligands and POMs (exptl,19.29%; calcd,19.12%). The TG curves of **3** and **4** showed a multistep weight loss: the first weight

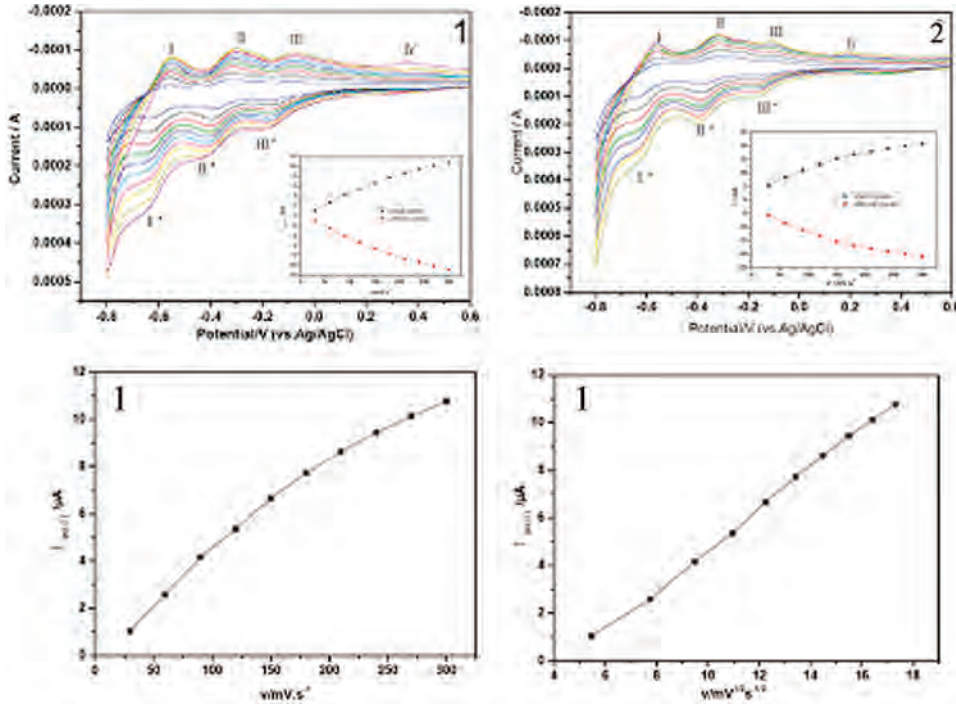

Figure 10. The cyclic voltammograms of the **1**-CPE (left) and **2**-CPE (right) in 1 M H_2SO_4 at the different scan rates (from inner to outer: 30, 60, 90, 120, 150,180, 210, 240, 270, and 300 mV·s^{-1}). The inset shows plots of the anodic and the cathodic peak currents of II−II′ against scan rates. The lower views show the cathodic peak II−II′ currents against scan rates and square roots of scan rates.

losses of 0.78% for **3** (calcd 0.75%) and 0.59% for **4** (calcd 0.54%) below 160 °C were assigned to the removal of H_2O, and the second continuous weight losses of 12.08% for **3** (calcd 11.94%) and 15.93% for **4** (calcd 16.33%) at *ca.* 340−630 °C may be ascribed to the decomposition of 4,4′-bipy ligands and POMs, respectively.

Electrochemical Properties. POMs have been exploited extensively in the electrocatalytic reductions by a chemically modified electrode (CME), because of the ability to undergo reversible multielectron redox processes.[26] However, due to the good solubility of the traditional CME with POMs, its application is limited.[27] The three-dimensional bulk-modified CPEs have been widely applied in electrochemistry with advantages: they are inexpensive, easy to handle, and easy to prepare. Herein, the electrochemical activities of **1**−**4** were investigated under identical conditions by using **1**-, **2**-, **3**-, and **4**-CPE.

Voltammetric Behavior of Compound-CPE in Aqueous Electrolytes. The cyclic voltammetric (CV) behaviors of CPEs were measured in the potential range +600 to −800 mV in a 1.0 M H_2SO_4 aqueous solution at different scan rates. As seen from Figure 10, it can be clearly seen that, in the potential range, three pairs of redox peaks (I−I′, II−II′, and III−III′) are observed for **1** and **2**, ascribed to three consecutive redox processes of W atoms, and the mean peak potentials $E_{1/2} = (E_{pc} + E_{pa})/2$ are −591, −352, and +120 mV for **1** and −596, −354, and +140 for **2**. It is also noted that there is an additional irreversible anodic peak (IV) for **1** and **2**, which should be assigned to the oxidation of Ag(I).[28] For the **3**- and **4**-CPE, three pairs of redox peaks of W atoms are also observed in the potential range (shown in Figures S6 and S7, Supporting Information), and the mean peak potentials $E_{1/2}$ are −600, −344, and +140 mV for **3** and −598, −354, and +133 for **4**. Although the same building blocks in compounds **1**−**4** are used, the mean peak potentials are slightly different, which are due to their different chemical environments. This fact suggests that POMs are the active center for electrochemical redox activity in CPEs. With the increase of scan rate, the increasing extent of the anodic and cathodic peak currents are almost the same, and the peak potentials change gradually: the cathodic peak potentials shift toward the negative direction and the corresponding anodic peak potentials to the positive direction, and the peak-to-peak separation between the corresponding cathodic and anodic peaks increases, but the average peak potentials do not change on the whole. When the scan rates are lower than 120 mV s^{-1}, the peak currents are proportional to the scan rates, which indicates that the redox process is surface-controlled, and the exchanging rate of the electrons is fast; however, when the scan rates are higher than 120 mV s^{-1}, the peak currents are proportional to the square root of the scan rate, which indicates that the redox process is diffusion-controlled.

Electrocatalytic Activity. As is known, POMs have been exploited extensively in electrocatalytic reductions. For example, Dong, Keita, and Toth and their respective coworkers have researched that Keggin POMs can be used as electrocatalysts for the reduction of nitrite and hydrogen

(26) (a) Xi, X.; Wang, G.; Liu, B.; Dong, S. *Electrochim. Acta* **1995**, *40*, 1025–1029. (b) Sadakane, M.; Steckhan, E. *Chem. Rev.* **1998**, *98*, 219–237.

(27) Wang, P.; Wang, X.; Zhu, N. Y. *Electrochim. Acta* **2000**, *46*, 637–641.

(28) Berchmans, S.; Nirmal, R. G.; Prabaharan, G.; Madhu, S.; Yegnaraman, V. *J. Colloid Interface Sci.* **2006**, *303*, 604–610.

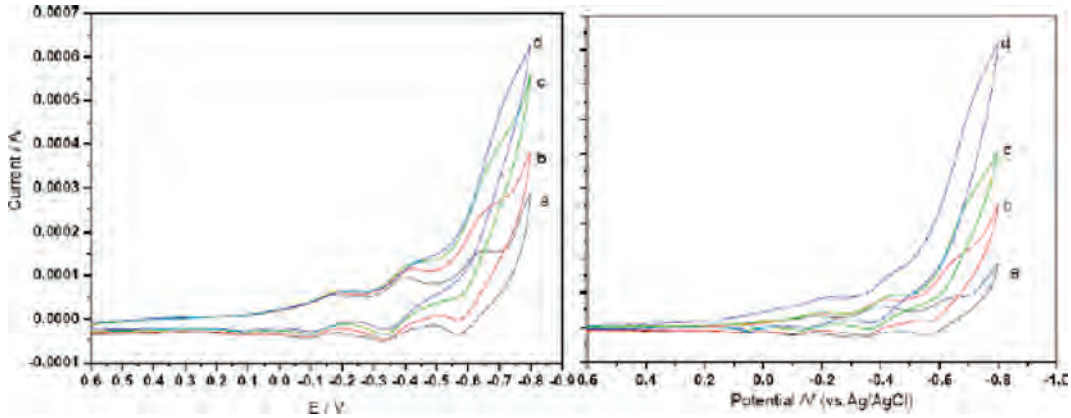

Figure 11. Cyclic voltammograms of **1**-CPE (left) and **2**-CPE (right) in 1 M H_2SO_4 containing 0 (a), 4 (b), 8 (c), and 12 (d) mM $KBrO_3$. Scan rate: 60 mV s^{-1}.

peroxide.[29] Herein, compounds **1** and **2** were employed to fabricate POM nanoparticle-modified electrodes to electrocatalyze the reduction of bromate and nitrite.

Figure 11 shows cyclic voltammograms for the electrocatalytic reduction of bromate at **1**- and **2**-CPE in a 1 M H_2SO_4 aqueous solution. **1**- and **2**-CPE present similar and good electrocatalytic activities for the reduction of bromate. It can be seen that, with the addition of bromate, the first and the second reduction peak currents increase gradually while the corresponding oxidation peak currents gradually decrease; however, the third redox peaks remain almost unchanged, which indicates that the four- and six-electron reduced species of P_2W_{18} anions present electrocatalytic activity. Owing to the high overpotential required at most electrode surfaces for the direct electroreduction of nitrite ions, no obvious response is observed for nitrite at bare CPE in the potential range. Figure S8 (Supporting Information) shows the cyclic voltammograms of **1**- and **2**-CPE in an acid solution containing nitrite. The result indicates that CPEs have good electrocatalytic activities in the reduction of nitrite. With the addition of nitrite, all three reduction peak currents increase, while the corresponding oxidation peak currents decrease, suggesting that the reduction of nitrite involves two-, four-, and six-electron-reduced species. It is noted that the six-electron-reduced species has the largest catalytic activity toward the reduction of nitrite.

Conclusion

By using Wells-Dawson POMs, Ag^+ ions, and 4,4′-bipy as building elements, two high-dimensional and high-connected Wells-Dawson POM-based compounds modified by TMCs were successfully obtained. Compound **2** possesses the highest coordination number and the richest coordination fashion of the Wells-Dawson POMs. The informative structures of compounds **1** and **2** indicate that the high-dimensional assembly of POM−TMC coordination polymers depends on a synergic effect of polyoxoanion templates, metal ion coordination geometries, and the steric hindrance of TMCs. In this work, we also systematically investigate the pH value effect on the structures of the Wells-Dawson POM-based coordination polymers. The result shows that the pH value of the reaction plays a key role in the structural control of self-assembled processes. On the basis of the Ag and acid−base chemistry, we explained the pH-dependence of the products. The work, to some extent, provides a good example of reasonable design and controllable assembly of POM-based coordination polymers.

Acknowledgment. This work is financially supported by the National Natural Science Foundation of China (20671016) and the Program for Changjiang Scholars and Innovative Research Team in University and the Analysis and Testing Foundation of Northeast Normal University.

Supporting Information Available: Tables of selected bond lengths (Å) and bond angles (deg) for compounds **1**−**4**; IR, TG, and CV data; and part structural figures of compounds **1**−**4**. This information is available free of charge via the Internet at http://pubs.acs.org.

IC702407Y

(29) (a) Keita, B.; Belhouari, A.; Nadjo, L.; Contant, R. *J. Electroanal. Chem.* **1995**, *381*, 243–250. (b) Toth, J. E.; Anson, F. C. *J. Electroanal. Chem.* **1988**, *256*, 361–370.